

Pervasive contingency and entrenchment in a billion years of Hsp90 evolution

Tyler N. Starr^{a,1}, Julia M. Flynn^{b,1}, Parul Mishra^{b,c,1}, Daniel N. A. Bolon^{b,2}, and Joseph W. Thornton^{d,e,2,3}

^aDepartment of Biochemistry and Molecular Biology, University of Chicago, Chicago, IL 60637; ^bDepartment of Biochemistry and Molecular Pharmacology, University of Massachusetts Medical School, Worcester, MA 01605; ^cDepartment of Animal Biology, School of Life Sciences, University of Hyderabad, 500046 Hyderabad, India; ^dDepartment of Ecology and Evolution, University of Chicago, Chicago, IL 60637; and ^eDepartment of Human Genetics, University of Chicago, Chicago, IL 60637

Edited by Eric A. Gaucher, Georgia Institute of Technology, Atlanta, GA, and accepted by Editorial Board Member Daniel L. Hartl March 12, 2018 (received for review October 17, 2017)

Interactions among mutations within a protein have the potential to make molecular evolution contingent and irreversible, but the extent to which epistasis actually shaped historical evolutionary trajectories is unclear. To address this question, we experimentally measured how the fitness effects of historical sequence substitutions changed during the billion-year evolutionary history of the heat shock protein 90 (Hsp90) ATPase domain beginning from a deep eukaryotic ancestor to modern *Saccharomyces cerevisiae*. We found a pervasive influence of epistasis. Of 98 derived amino acid states that evolved along this lineage, about half compromise fitness when introduced into the reconstructed ancestral Hsp90. And the vast majority of ancestral states reduce fitness when introduced into the extant *S. cerevisiae* Hsp90. Overall, more than 75% of historical substitutions were contingent on permissive substitutions that rendered the derived state nondeleterious, became entrenched by subsequent restrictive substitutions that made the ancestral state deleterious, or both. This epistasis was primarily caused by specific interactions among sites rather than a general effect on the protein's tolerance to mutation. Our results show that epistasis continually opened and closed windows of mutational opportunity over evolutionary timescales, producing histories and biological states that reflect the transient internal constraints imposed by the protein's fleeting sequence states.

epistasis | ancestral protein reconstruction | molecular evolution | protein evolution | heat shock proteins

Epistatic interactions can, in principle, affect the sequence changes that accumulate during evolution. A deleterious mutation's expected fate is to be purged by purifying selection, but it can be fixed if a permissive substitution renders it neutral or beneficial (1–3). Conversely, a neutral mutation—which by definition is initially reversible to the ancestral state without fitness cost—may become entrenched by a subsequent restrictive substitution that renders the ancestral state deleterious (1, 4, 5); reversal of the entrenched mutation would then be unlikely unless the restrictive substitution were itself reversed or another permissive substitution occurred.

The extent to which epistasis-induced contingency and entrenchment actually affected protein sequence evolution is unclear, because there is no consensus on the prevalence, effect size, or mechanisms of epistasis among historical substitutions. Deep mutational scans have revealed frequent epistasis among the many possible mutations within proteins (6–10), but how these interactions affect the substitutions that actually occurred during historical evolution is not known. Historical case studies have shown that particular substitutions were contingent (3, 11–13) or became entrenched during evolution (5), but the generality of these phenomena is unknown. Computational approaches suggest pervasive contingency and entrenchment among substitutions (1, 4, 14–18), but some of these analyses rely on models of uncertain adequacy (19–21), and their claims have not been experimentally validated. Swapping sequence states among extant orthologs has revealed frequent epistasis among substitutions (22), but this “horizontal” approach, unpolarized

with respect to time, leaves unresolved whether permissive or restrictive interactions are at play (23). Some experimental studies have systematically examined epistasis among substitutions in an historical context, but most have measured effects on protein function (2, 22) or stability (20, 24), leaving unexamined the prevalence of epistasis with respect to fitness—the phenotype that directly affects evolutionary fate. Others have focused on fitness but used methods that cannot detect effects of relatively small magnitude, which could be widespread and consequential for evolutionary processes (2, 25).

We directly evaluated the roles of contingency and entrenchment on historical sequence evolution by precisely quantifying changes over time in the fitness effects of all substitutions that accumulated during the long-term evolution of heat shock protein 90 (Hsp90) from a deep eukaryotic ancestor to *Saccharomyces cerevisiae*. Hsp90 is an essential molecular chaperone that facilitates folding and regulation of substrate proteins through an ATP-dependent cycle of conformational changes, modulated by cochaperone proteins. Orthologs from other fungi, animals, and

Significance

When mutations within a protein change each other's functional effects—a phenomenon called epistasis—the paths available to evolution at any moment in time depend on the specific set of changes that previously occurred in the protein. The extent to which epistasis has shaped historical evolutionary trajectories is unknown. Using a high-precision bulk fitness assay and ancestral protein reconstruction, we measured the fitness effects in ancestral and extant sequences of all historical substitutions that occurred during the billion-year trajectory of an essential protein. We found that most historical substitutions were contingent on prior epistatic substitutions and/or entrenched by subsequent changes. These results establish that epistasis caused widespread, consequential shifts in the site-specific fitness constraints that shaped the protein's historical trajectory.

Author contributions: T.N.S., J.M.F., P.M., D.N.A.B., and J.W.T. designed research; T.N.S., J.M.F., and P.M. performed research; T.N.S., J.M.F., and P.M. analyzed data; and T.N.S. and J.W.T. wrote the paper.

The authors declare no conflict of interest.

This article is a PNAS Direct Submission. E.A.G. is a guest editor invited by the Editorial Board.

Published under the PNAS license.

Data deposition: The data reported in this paper have been deposited in the National Center for Biotechnology Information Sequence Read Archive (SRA), <https://www.ncbi.nlm.nih.gov/sra> (accession no. SRP126524). Processed sequencing data and scripts to reproduce all analyses are available at https://github.com/JoeThorntonLab/Hsp90_contingency-entrenchment.

¹T.N.S., J.M.F., and P.M. contributed equally to this work.

²D.N.A.B. and J.W.T. contributed equally to this work.

³To whom correspondence should be addressed. Email: joet1@uchicago.edu.

This article contains supporting information online at www.pnas.org/lookup/suppl/doi:10.1073/pnas.1718133115/-DCSupplemental.

occurred not only along the trajectory from ancAmoHsp90 to ScHsp90 but also in parallel on another fungal lineage; in both cases, candidate epistatic substitution i378L co-occurred on the same branch (Fig. S9 *A* and *B*). As predicted if i378L entrenched f23V, we found that introducing the ancestral state i378 in ScHsp90 relieves the deleterious effect of the ancestral state f23 (Fig. 4*A*). These two residues directly interact in the protein's tertiary structure to position a key residue in the ATPase active site (Fig. S9 *C* and *D*), explaining their specific epistatic interaction.

In the case of E7a—the other reversion strongly deleterious in ScHsp90—the ancestral state was reacquired in a closely related fungal lineage. We reasoned that the substitutions that entrenched a7E on the lineage leading to ScHsp90 must have themselves reverted or been further modified on the fungal branch in which reversal E7a occurred. We identified two candidates (n13T and a151N) that met these criteria (Fig. S10 *A–C*). As predicted, experimentally introducing the ancestral states n13 or a151 into ScHsp90 relieves much of the fitness defect caused by the ancestral state a7, indicating that substitutions n13T and a151N entrenched a7E (Fig. 4*B*). These three sites are on interacting secondary structural elements that are conformationally rearranged when Hsp90 converts between ADP- and ATP-bound states (Fig. S10 *D* and *E*).

To test whether these states specifically restrict particular substitutions or are general epistatic modifiers, we asked whether the restrictive substitutions that entrenched one substitution also entrenched the other (2). As predicted if the interactions among these sets of substitutions are specific, introducing L378i does not ameliorate the fitness defect caused by E7a, and introducing T13n or N151a does not ameliorate the fitness defect caused by V23f (Fig. 4 *C* and *D*). These data indicate that specific biochemical mechanisms underlie these large-effect restrictive interactions.

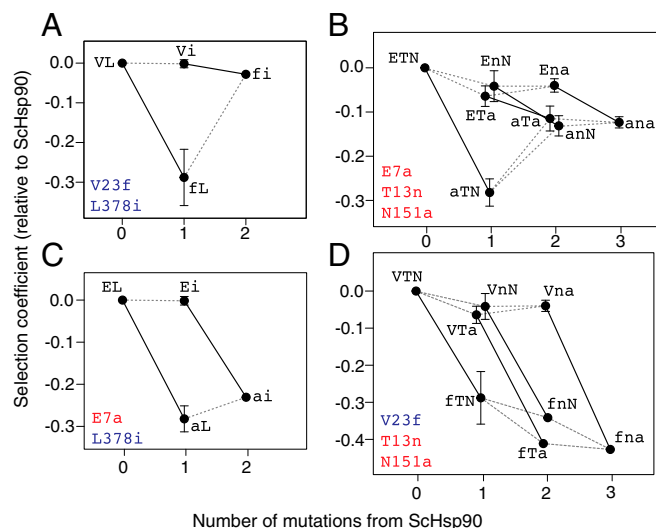


Fig. 4. Epistatic interactions are specific. Large-effect deleterious reversions and restrictive substitutions that contributed to their irreversibility. For each single, double, or triple mutant in ScHsp90, the selection coefficient relative to ScHsp90 is shown, as assessed in monoculture growth assays. Lines connect genotypes that differ by a single mutation; solid lines indicate the effect of the large-effect reversions in each background. Error bars, SEM for two to four replicates (SI Methods) (absence of error bar indicates one replicate). Data points are labeled by amino acid states: lowercase, ancestral state; uppercase, derived state. Mutations tested in each cycle are in the Bottom Left corner; those in the same color interact specifically with each other. (A) Deleterious reversion V23f is ameliorated by L378i. (B) Deleterious reversion E7a is partially ameliorated by N151a or T13n. (C) L378i does not ameliorate E7a. (D) N151a and T13n do not ameliorate V23f.

Finally, we investigated whether the epistatic interactions among the set of small-effect substitutions in this trajectory are also specific or the nonspecific result of a threshold-like relationship between fitness and some bulk property such as stability (2, 35). If epistasis is mediated by a nonspecific threshold relationship, mutations that decrease fitness in one background will never be beneficial in another, although they can be neutral if buffered by the threshold (Fig. 5*A*) (2, 20, 25). In contrast, specific epistatic interactions can switch the sign of a mutation's selection coefficient in different sequence contexts (Fig. 5*B*) (37). As predicted for specific epistasis, we found that for most differences between ancAmoHsp90 and ScHsp90 (65%), the ancestral state confers increased fitness relative to the derived state in the ancestral background but decreases it in the extant background (Fig. 5*C*). The selection coefficients of mutations are negatively correlated between backgrounds ($P = 0.009$), indicating that the substitutions that became most entrenched in the present also required the strongest permissive effect in the past. This pattern is expected if the structural constraints that determine the selective cost of having a suboptimal state at some site are conserved over time, but the specific state that is preferred depends on the residues present at other sites.

Taken together, these findings indicate that most epistasis during the long-term evolution of Hsp90 involved specific one-to-one (or few-to-few) interactions among sites, not general effects on the protein's tolerance to mutation.

Discussion

Relation to Prior Work. We observed widespread and specific epistasis over the course of a billion years of Hsp90 evolution, during which the protein's function, physical architecture, and fitness were conserved. The fraction of historical substitutions that were contingent on permissive substitutions, entrenched by restrictive substitutions, or both—about 80%—is considerably higher than suggested by previous experimental work (2, 22, 24) and some computational analyses (14), rivaling the highest estimates from computational studies (1, 16, 17). One explanation for the more widespread epistatic interactions in our study may be our method's capacity to detect much smaller growth deficits than have been discernable in previous experimental studies.

Another difference from previous research is that we primarily observed specific epistasis, whereas several studies have found a dominant role for nonspecific stability-mediated epistasis, particularly during the short-term evolution of viruses (2, 11, 20). This disparity could be attributable to a difference in selective regime or in timescale: the epistatic constraints caused by specific interactions are expected to be maintained over far longer periods of time than those caused by nonspecific interactions, which are easily replaced by other substitutions because of the many-to-many relationship between permissive and permitted amino acid states (2, 20, 37). The prevalence and type of epistasis may also vary because of differences in proteins' physical architectures. Additional case studies will be necessary to evaluate the causal role of these and other factors in determining the nature of epistatic interactions during evolution.

Limitations. Our strategy has some known limitations, but none is likely to change our major conclusions. For example, we assayed the effect of long-past substitutions in the context of extant yeast cells. But our experiments indicate that there is only very weak epistasis for fitness between historical substitutions within Hsp90 and those at other loci, because the reconstructed ancestral Hsp90 chimeras cause a fitness deficit of only 0.01–0.04 when introduced into *S. cerevisiae* cells—much smaller than the sum of intramolecular incompatibilities revealed by introducing the ancestral states individually. Our finding of widespread contingency and entrenchment is therefore not an artifact

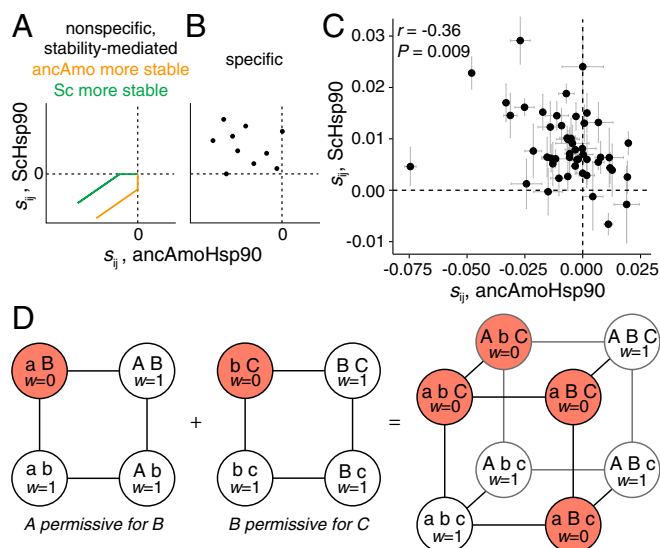


Fig. 5. A daisy-chain model of specific epistasis. (A and B) Expected relationship under two models of epistasis between selection coefficients of ancestral-to-derived mutations (s_{ij}) when introduced into ancestral (x axis) or derived (y axis) backgrounds. (A) Nonspecific epistasis: if genetic interactions are the nonspecific result of a threshold-like, buffering relationship between stability (or another bulk property) and fitness (2, 35), then the effects of strongly deleterious mutations will be positively correlated between the two backgrounds, but weakly deleterious mutations in the less stable background may be neutral in the more stable background (yellow, ancAmoHsp90 more stable; green, ScHsp90 more stable). (B) Specific epistasis: if interactions reflect specific couplings between sites, then mutations from ancestral to derived states can be deleterious in the ancestral background but beneficial in the derived background, occupying the upper left quadrant of the plot. (C) Measured selection coefficients for ancestral-derived state pairs that differ between ancAmoHsp90 and ScHsp90. Dashed lines, $s = 0$. Error bars, SEM from two replicate bulk competition measurements. r , Pearson correlation coefficient and associated P value. Full distribution showing strongly deleterious outliers in the ScHsp90 or ancAmoHsp90 data are shown in Fig. S10F. (D) Daisy-chain model of specific epistatic interactions. Each square shows the mutant cycle for a pair of substitutions (A and B or B and C; lowercase, ancestral state; uppercase, derived), one of which is permissive for the other. Each circle is a genotype colored by its fitness (w): white, neutral; red, deleterious. Edges are single-site amino acid changes. The cube shows the combined mutant cycle for all three substitutions. Permissive substitutions become entrenched when the mutation that was contingent upon it occurs. Substitutions in the middle of the daisy chain, which require a permissive mutation and are permissive for a subsequent mutation, are both contingent and entrenched.

of incompatibilities between ancestral Hsp90 states and the genotype of present-day *S. cerevisiae* at other loci.

A second potential limitation is that the ancestral states we tested were reconstructed phylogenetically, not known empirically. But the vast majority of states were inferred with high statistical confidence, because the Hsp90 NTD is well conserved and we used a densely sampled alignment. The ambiguity that was present primarily concerned the specific ancestral node at which an inferred ancestral state was present, not whether or not it was ancestral somewhere along the trajectory, which is the key inference for our purposes. Even when all states with any degree of statistical uncertainty in the ancestral reconstruction were excluded from the analysis, the remaining data strongly supported our conclusions concerning contingency and entrenchment.

Finally, we measured fitness under a particular set of experimental conditions. Our assay system reduces Hsp90 expression to ~1% of the endogenous level (30). Based on previous work quantifying the relationship between Hsp90 function, expression, and growth rate (30), we estimate that the average selection coefficient of -0.01 we observed among contingent or entrenched substitutions corresponds to a fitness deficit of approximately

$s = -5 \times 10^{-6}$ under native-like expression levels. Mutations with selection coefficients in this range would likely be subject to purifying selection in large microbial populations (39–41). Our assay also tests fitness under log-phase growth conditions in rich media. A more heterogeneous or demanding environment would likely increase the magnitude of selective effects of Hsp90 mutations, because stress should amplify the fitness consequences of mutations in the proteostasis machinery.

Implications. Our observation that contingency and entrenchment affected the majority of historical substitutions suggests a daisy-chain model by which genetic interactions structured long-term Hsp90 evolution (Fig. 5D). A permissive mutation becomes entrenched and irreversible once a substitution contingent upon it occurs; if the contingent substitution subsequently permits a third substitution, it too becomes entrenched (1, 16).

Most of the substitutions along the trajectory from ancAmoHsp90 to ScHsp90 were both contingent and entrenched, suggesting that they occupy an internal position in this daisy chain. Each of these changes closed reverse paths at some sites and opened forward paths at others, which, if taken, would then entrench the previous step. Evolving this way over long periods of time, proteins come to appear exquisitely well-adapted to the conditions of their existence, with most present states superior to past ones. But the conditions that make today's states so fit include—or are even dominated by—the transient internal organization of the protein itself.

Methods

For additional details, see *SI Methods*.

Phylogenetic Inference and Ancestral Reconstruction. We inferred the ML phylogeny for 261 Hsp90 protein sequences from the Amorphea clade, with Viridiplantae as an outgroup, under the LG+Γ+F model in RAXML, version 8.1.17 (42). Most probable ancestral NTD sequences were reconstructed on this ML phylogeny using the AAML module of PAML, version 4.4 (43). The trajectory of sequence change was enumerated from the amino acid sequence differences between successive ancestral nodes on the lineage from the common ancestor of Amorphea (ancAmoHsp90) to *S. cerevisiae* Hsp82 (ScHsp90). Ancestral states are defined as amino acid states not present in ScHsp90 that occurred in at least one ancestral node on the lineage from ancAmoHsp90 to ScHsp90. Derived states are defined as amino acid states not present in the reconstructed ancAmoHsp90 sequence that occurred in at least one descendent node on the lineage to ScHsp90.

Bulk Growth Competitions. The ScHsp90 and ancAmoHsp90 NTD (+L378i; *SI Methods* and Fig. S2D) protein-coding sequences were expressed together with the other domains from ScHsp90 from the p414ADHΔTer plasmid (30). Individual mutations in each variant library were introduced via PCR. Library genotypes were tagged with short barcodes to simplify sequencing steps during the bulk competition (44); barcodes were associated with variant genotypes via paired-end sequencing on an Illumina MiSeq instrument. Variant libraries were transformed into the DBY288 Hsp90 *S. cerevisiae* shutoff strain (45, 46) and grown for 48 h (ScHsp90 library) or 31 h (ancAmoHsp90 library) under selective conditions. Cultures were maintained in log phase by regular dilution with fresh media, maintaining a population size of 10^9 or greater, and samples of $\sim 10^8$ cells were collected at regular time points over the course of the bulk competition. Plasmid DNA was isolated from each time point (47), and the frequency of each library genotype at each time point was determined via Illumina sequencing. Bulk competitions were performed in duplicate.

Determination of Selection Coefficients. The ratio of the frequency of each variant in the library relative to wild type (ancAmoHsp90 or ScHsp90) was determined from the number of sequence reads at each time point, and the slope of the logarithm of this ratio versus time (in number of generations) was determined as the raw per-generation selection coefficient (s) (48):

$$s = d/dt[\ln(n_m/n_{wt})],$$

where n_m and n_{wt} are the number of sequence reads of mutant and wild type, respectively, and time is measured in number of wild-type generations. For genotypes that were not assayed in the bulk competition, selection

coefficients were determined from monoculture growth rates (48), measured over 30 h of growth with periodic dilution to maintain log-phase growth (30). Selection coefficients for both types of measurement were scaled in relative fitness space ($w = e^s$) such that an Hsp90 null allele, which is lethal, has a relative fitness of 0 ($s = -\infty$).

Estimating the Fraction of Deleterious Mutations. We estimated the fraction of mutations in each library that are deleterious by fitting the distribution of mutant selection coefficients to a mixture model of underlying Gaussian distributions. One of the underlying mixture components was required to have the mean and SD estimated from replicate measurements of wild-type sequences present in the library but represented by independent barcodes; remaining mixture components had a freely fit mean and SD, and all components had a freely fit mixture proportion. The optimal number of mixture components was determined via Akaike information criterion. The mixture component derived from the wild-type sampling distribution was taken to represent neutral mutations in the library, and the other mixture components were taken to reflect nonneutral mutations. We estimated the fraction of neutral mutations as the mixture proportion of the neutral mixture component. We then estimated the proportion of deleterious (or beneficial) mutations as the sum of the weighted cumulative density of all nonneutral components that was below (or above) zero.

To determine the robustness of the mixture model's estimates of the fraction of deleterious (or beneficial) mutations, we used three other approaches to analyze the distribution of fitness measurements. The simplest, a nonparametric approach, estimates the proportion of deleterious (or beneficial) mutations as the proportion of mutations with observed selection

coefficients less (or greater) than 0. The second approach is an empirical Bayes approach that calculates the posterior probability that each mutation is deleterious (or beneficial), given the experimentally observed selection coefficients and measurement error for wild-type and mutant genotypes; these posterior probabilities are summed to yield the estimated proportion of mutations in each fitness category. Third, we constructed 95% CIs for each mutation's selection coefficient given its mean over two replicates and SE estimated over all mutations and counted the number of mutations with selection coefficients less (or greater) than zero whose CIs do not overlap zero.

Data and Code Availability. Processed sequencing data and scripts to reproduce all analyses are available at https://github.com/JoeThorntonLab/Hsp90_contingency-entrenchment. Tables listing mutants and their selection coefficients are included as [Datasets S5](#) and [S6](#). Raw sequencing data from each bulk competition have been deposited in the National Center for Biotechnology Information Sequence Read Archive under accession number SRP126524. Tables linking barcode variants to their associated Hsp90 genotype are included as [Datasets S7](#) and [S8](#).

ACKNOWLEDGMENTS. We thank members of the J.W.T. laboratory for comments on the manuscript and Jeff Boucher for technical assistance. This work was supported by National Institutes of Health Grants R01GM104397 and R01GM121931 (to J.W.T.), R01GM112844 (to D.N.A.B.), F32GM119205-2 (to J.M.F.), and T32-GM007183 (to T.N.S.); Government of India Department of Biotechnology Ramalingaswami Fellowship (to P.M.); and a National Science Foundation Graduate Research Fellowship (to T.N.S.).

- Shah P, McCandlish DM, Plotkin JB (2015) Contingency and entrenchment in protein evolution under purifying selection. *Proc Natl Acad Sci USA* 112:E3226–E3235.
- Gong LI, Suchard MA, Bloom JD (2013) Stability-mediated epistasis constrains the evolution of an influenza protein. *eLife* 2:e00631.
- Ortlund EA, Bridgham JT, Redinbo MR, Thornton JW (2007) Crystal structure of an ancient protein: evolution by conformational epistasis. *Science* 317:1544–1548.
- Pollock DD, Thiltgen G, Goldstein RA (2012) Amino acid coevolution induces an evolutionary Stokes shift. *Proc Natl Acad Sci USA* 109:E1352–E1359.
- Bridgham JT, Ortlund EA, Thornton JW (2009) An epistatic ratchet constrains the direction of glucocorticoid receptor evolution. *Nature* 461:515–519.
- Olson CA, Wu NC, Sun R (2014) A comprehensive biophysical description of pairwise epistasis throughout an entire protein domain. *Curr Biol* 24:2643–2651.
- Bank C, Hietpas RT, Jensen JD, Bolon DNA (2015) A systematic survey of an intragenic epistatic landscape. *Mol Biol Evol* 32:229–238.
- Podgornaia AI, Laub MT (2015) Protein evolution. Pervasive degeneracy and epistasis in a protein-protein interface. *Science* 347:673–677.
- Melamed D, Young DL, Gamble CE, Miller CR, Fields S (2013) Deep mutational scanning of an RRM domain of the *Saccharomyces cerevisiae* poly(A)-binding protein. *RNA* 19:1537–1551.
- Sarkisyan KS, et al. (2016) Local fitness landscape of the green fluorescent protein. *Nature* 533:397–401.
- Bloom JD, Gong LI, Baltimore D (2010) Permissive secondary mutations enable the evolution of influenza oseltamivir resistance. *Science* 328:1272–1275.
- Natarajan C, et al. (2016) Predictable convergence in hemoglobin function has unpredictable molecular underpinnings. *Science* 354:336–339.
- McKeown AN, et al. (2014) Evolution of DNA specificity in a transcription factor family produced a new gene regulatory module. *Cell* 159:58–68.
- Soylemez O, Kondrashov FA (2012) Estimating the rate of irreversibility in protein evolution. *Genome Biol Evol* 4:1213–1222.
- Jordan DM, et al.; Task Force for Neonatal Genomics (2015) Identification of *cis*-suppression of human disease mutations by comparative genomics. *Nature* 524:225–229.
- Povolotskaya IS, Kondrashov FA (2010) Sequence space and the ongoing expansion of the protein universe. *Nature* 465:922–926.
- Breen MS, Kemena C, Vlasov PK, Notredame C, Kondrashov FA (2012) Epistasis as the primary factor in molecular evolution. *Nature* 490:535–538.
- Goldstein RA, Pollard ST, Shah SD, Pollock DD (2015) Nonadaptive amino acid convergence rates decrease over time. *Mol Biol Evol* 32:1373–1381.
- McCandlish DM, Rajon E, Shah P, Ding Y, Plotkin JB (2013) The role of epistasis in protein evolution. *Nature* 497:E1–E2; discussion E2–E3.
- Ashenberg O, Gong LI, Bloom JD (2013) Mutational effects on stability are largely conserved during protein evolution. *Proc Natl Acad Sci USA* 110:21071–21076.
- Mendes FK, Hahn Y, Hahn MW (2016) Gene tree discordance can generate patterns of diminishing convergence over time. *Mol Biol Evol* 33:3299–3307.
- Lunzer M, Golding GB, Dean AM (2010) Pervasive cryptic epistasis in molecular evolution. *PLoS Genet* 6:e1001162.
- Hochberg GKA, Thornton JW (2017) Reconstructing ancient proteins to understand the causes of structure and function. *Annu Rev Biophys* 46:247–269.
- Risso VA, et al. (2015) Mutational studies on resurrected ancestral proteins reveal conservation of site-specific amino acid preferences throughout evolutionary history. *Mol Biol Evol* 32:440–455.
- Doud MB, Ashenberg O, Bloom JD (2015) Site-specific amino acid preferences are mostly conserved in two closely related protein homologs. *Mol Biol Evol* 32:2944–2960.
- Piper PW, et al. (2003) Yeast is selectively hypersensitized to heat shock protein 90 (Hsp90)-targeting drugs with heterologous expression of the human Hsp90 α , a property that can be exploited in screens for new Hsp90 chaperone inhibitors. *Gene* 302:165–170.
- Wider D, Péli-Gulli M-P, Briand P-A, Tatu U, Picard D (2009) The complementation of yeast with human or *Plasmodium falciparum* Hsp90 confers differential inhibitor sensitivities. *Mol Biochem Parasitol* 164:147–152.
- Hietpas RT, Jensen JD, Bolon DNA (2011) Experimental illumination of a fitness landscape. *Proc Natl Acad Sci USA* 108:7896–7901.
- Adl SM, et al. (2012) The revised classification of eukaryotes. *J Eukaryot Microbiol* 59:429–493.
- Jiang L, Mishra P, Hietpas RT, Zeldovich KB, Bolon DNA (2013) Latent effects of Hsp90 mutants revealed at reduced expression levels. *PLoS Genet* 9:e1003600.
- McCandlish DM, Shah P, Plotkin JB (2016) Epistasis and the dynamics of reversion in molecular evolution. *Genetics* 203:1335–1351.
- Taylor JW, Berbee ML (2006) Dating divergences in the Fungal Tree of Life: review and new analyses. *Mycologia* 98:838–849.
- Eme L, Sharpe SC, Brown MW, Roger AJ (2014) On the age of eukaryotes: evaluating evidence from fossils and molecular clocks. *Cold Spring Harb Perspect Biol* 6:a016139.
- Ali MMU, et al. (2006) Crystal structure of an Hsp90-nucleotide-p23/Sba1 closed chaperone complex. *Nature* 440:1013–1017.
- Tokuriki N, Tawfik DS (2009) Stability effects of mutations and protein evolvability. *Curr Opin Struct Biol* 19:596–604.
- Harms MJ, Thornton JW (2013) Evolutionary biochemistry: revealing the historical and physical causes of protein properties. *Nat Rev Genet* 14:559–571.
- Starr TN, Thornton JW (2016) Epistasis in protein evolution. *Protein Sci* 25:1204–1218.
- Sailer ZR, Harms MJ (2017) Detecting high-order epistasis in nonlinear genotype-phenotype maps. *Genetics* 205:1079–1088.
- Tsai IJ, Bensasson D, Burt A, Koufopanou V (2008) Population genomics of the wild yeast *Saccharomyces paradoxus*: Quantifying the life cycle. *Proc Natl Acad Sci USA* 105:4957–4962.
- Peris D, et al. (2014) Population structure and reticulate evolution of *Saccharomyces eubayanus* and its lager-brewing hybrids. *Mol Ecol* 23:2031–2045.
- Almeida P, et al. (2015) A population genomics insight into the Mediterranean origins of wine yeast domestication. *Mol Ecol* 24:5412–5427.
- Stamatakis A (2014) RAxML version 8: a tool for phylogenetic analysis and post-analysis of large phylogenies. *Bioinformatics* 30:1312–1313.
- Yang Z, Kumar S, Nei M (1995) A new method of inference of ancestral nucleotide and amino acid sequences. *Genetics* 141:1641–1650.
- Hiatt JW, Patwardhan RP, Turner EH, Lee C, Shendure J (2010) Parallel, tag-directed assembly of locally derived short sequence reads. *Nat Methods* 7:119–122.
- Hietpas RT, Bank C, Jensen JD, Bolon DNA (2013) Shifting fitness landscapes in response to altered environments. *Evolution* 67:3512–3522.
- Mishra P, Flynn JM, Starr TN, Bolon DNA (2016) Systematic mutant analyses elucidate general and client-specific aspects of Hsp90 function. *Cell Reports* 15:588–598.
- Hietpas R, Roscoe B, Jiang L, Bolon DNA (2012) Fitness analyses of all possible point mutations for regions of genes in yeast. *Nat Protoc* 7:1382–1396.
- Chevin LM (2011) On measuring selection in experimental evolution. *Biol Lett* 7:210–213.

Supporting Information

Starr et al. 10.1073/pnas.1718133115

SI Methods

Phylogenetic Analysis and Ancestral Reconstruction. We obtained Hsp90 protein sequences from the Amorphea clade (1) from the National Center for Biotechnology Information, the Joint Genome Institute Fungal Genomics Program, the Broad Institute Multicellularity Project, the literature (2), and Iñaki Ruiz-Trillo, Institute of Evolutionary Biology, CSIC–Universitat Pompeu Fabra, Barcelona. Sequences are listed in Dataset S1; corresponding identifiers and sources of sequences are listed in Dataset S3. Each protein was used as a query in a BLASTp search against the human proteome to identify and retain Hsp90A orthologs. We used CD-HIT (3) to filter proteins with high sequence similarity. We removed sequences with >67% missing characters and highly diverged, unalignable sequences. Remaining sequences were aligned with Clustal Omega (4). Lineage-specific insertions were removed, as were unalignable linker regions (ScHsp90 sites 1–3, 225–237, 686–701). We added six Hsp90A sequences from Viridiplantae as an outgroup, resulting in a final alignment of 267 protein sequences and 680 sites (Dataset S1).

We inferred the maximum-likelihood (ML) phylogeny (Dataset S2) given our alignment and the LG model (5) with gamma-distributed among-site rate variation (four categories) and ML estimates of amino acid frequencies, which was the best-fit model as judged by Akaike information criterion (AIC). The phylogeny was inferred using RAXML, version 8.1.17 (6). The ML phylogeny reproduces accepted relationships between major taxonomic lineages (1, 7–11). Most probable ancestral sequences (Dataset S4) were reconstructed on the ML phylogeny using the AAML module of PAML, version 4.4 (12), given the alignment, ML phylogeny, and LG+ Γ model. The trajectory of sequence change was enumerated from the amino acid sequence differences between successive ancestral nodes on the lineage from the common ancestor of Amoebozoa + Opisthokonta (ancAmorphea) to *Saccharomyces cerevisiae* Hsp82 (ScHsp90, Uniprot P02829).

Coding sequences for the most probable ancestral amino acid sequences of the Hsp90 N-terminal domain (NTD) from ancAmorphea (ancAmoHsp90) and the common ancestor of Ascomycota yeast (ancAscoHsp90) were synthesized by IDT (Dataset S9). These sequences were cloned as chimeras with the ScHsp90 middle and C-terminal domains and intervening linkers via Gibson Assembly. AncAmoHsp90 also carries an additional reversion to the ancAmorphea state at site 378 in the middle domain (Fig. S2D), which is part of a loop that extends down and interacts with ATP and the NTD (13, 14).

Generating Mutant Libraries. ScHsp90 and ancAmoHsp90 gene constructs were expressed from the p414ADH Δ Ter plasmid (15). The ScHsp90 library consists of variants of the ScHsp90 NTD, each containing one mutation to an ancestral amino acid state. The ancAmoHsp90 library consists of variants of the ancAmoHsp90 NTD, each containing one mutation to a derived state. Two sets of PCR primers were designed for each mutation, to amplify Hsp90 NTD fragments N-terminal and C-terminal to the mutation of interest; primers introduce the mutation of interest and generate a 25-bp overlap between fragments, as well as 20-bp overlaps between each fragment and the destination vector for gene reassembly (Dataset S9). PCR was conducted with Pfu Turbo polymerase (Agilent) for 15 amplification cycles. The resulting PCR fragments were stitched together with a 10-cycle assembly PCR, pooled, and combined via Gibson Assembly (NEB) with a linearized p414ADH Δ Ter Hsp90 destination vector excised of the NTD.

Barcode Labeling of Library Genotypes. Following construction of the plasmid libraries, each variant in the library was tagged with a unique barcode to simplify sequencing steps during bulk competition (16). A pool of DNA constructs containing a randomized 18-bp barcode sequence (N18) and Illumina sequencing primer annealing regions (IDT; Dataset S9) was cloned 200 nt downstream from the hsp90 stop codon via restriction digestion, ligation, and transformation into chemically competent *Escherichia coli*. Cultures with different amounts of the transformation reaction were grown overnight and the colony-forming units in each culture were assessed by plating a small fraction. We isolated DNA from the transformation that contained ~10- to 20-fold more colony-forming units than mutants, with the goal that each mutant would be represented by 10–20 unique barcodes.

To associate barcodes with Hsp90 mutant alleles, we conducted paired-end sequencing of each library using primers that read the N18 barcode in the first read and the Hsp90 NTD in the other (Dataset S9). To generate short DNA fragments from the plasmid library that would be efficiently sequenced, we excised the gene region between the NTD and the N18 barcode via restriction digest, followed by blunt ending with T4 DNA polymerase (NEB) and plasmid ligation at a low concentration (3 ng/ μ L) to favor circularization over bimolecular ligations. The resulting DNA was religated by restriction digest, and Illumina adapter sequences were added via an 11-cycle PCR (Dataset S9). The resulting PCR products were sequenced using an Illumina MiSeq instrument with asymmetric reads of 50 bases and 250 bases for Read1 and Read2, respectively. After filtering low-quality reads (Phred scores < 10), the data were organized by barcode sequence. For each barcode that was read more than three times, we generated a consensus sequence of the N domain indicating the mutation that it contained (Datasets S7 and S8).

Bulk Growth Competitions. For bulk fitness assessments, we transformed *S. cerevisiae* with the ScHsp90 library along with wild-type ScHsp90 and a no-insert control; we also transformed *S. cerevisiae* with the ancAmoHsp90 library along with wild-type ScHsp90, wild-type ancAmoHsp90, and a no-insert control. Concentrations of plasmids were adjusted to yield a 2:6:1 molar ratio of wild type/no-insert control/average variant in the library. Plasmid libraries and corresponding controls were transformed into the DBY288 Hsp90 shutoff strain (17, 18), resulting in ~150,000 unique yeast transformants representing 50-fold sampling for the average barcode. Following recovery, transformed cells were washed five times in SRGal-W (synthetic 1% raffinose and 1% galactose lacking tryptophan) media to remove extracellular DNA, and then transferred to plasmid selection media SRGal-W and grown at 30 °C for 48 h with repeated dilution to maintain the cells in log phase of growth. To select for function of the plasmid-borne Hsp90 allele, cells were shifted to shutoff conditions by centrifugation, washing, and resuspension in 200 mL of synthetic 2% dextrose lacking tryptophan (SD-W) media and ampicillin (50 μ g/mL), and grown at 30 °C, 225 rpm. Following a 16-h growth period required to shut off expression of the wild-type chromosomal Hsp90, we collected samples of ~10⁸ cells at eight or more time points over the course of 48 h (ScHsp90 library) or 31 h (ancAmoHsp90 library) and stored them at –80 °C. Cultures were maintained in log phase by regular dilution with fresh media, maintaining a population size of 10⁹ or greater throughout the bulk competition. Bulk competitions of each library were conducted in duplicate from independent transformations.

DNA Preparation and Sequencing. We collected plasmid DNA from each bulk competition time point as previously reported (19). Purified plasmid was linearized with *AscI*. Barcodes were amplified by 18 cycles of PCR using Phusion polymerase and primers that add Illumina adapter sequences, as well as an 8-bp identifier used to distinguish among libraries and time points (Dataset S9). Identifiers were designed so that each differed by more than two bases from all others to avoid misattributions due to sequencing errors. PCR products were purified two times over silica columns (Zymo Research), and quantified using the KAPA SYBR FAST qPCR Master Mix (Kapa Biosystems) on a Bio-Rad CFX machine. Samples were pooled and sequenced on an Illumina NextSeq (ancAmoHsp90 library) or HiSeq 2000 (ScHsp90 library) instrument in single-end 100-bp mode.

Analysis of Bulk Competition Sequencing Data. Illumina sequence reads were filtered for Phred scores >20, strict matching of the sequence of the intervening bases to the template, and strict matching of the N18 barcode and experimental identifier to those that were expected in the given library. Reads that passed these filters were parsed based on the identifier sequence. For each identifier, the data were condensed by generating a count of each unique N18 read. The unique N18 count file was then used to identify the frequency of each mutant using the variant-barcode association table. For each variant in the library, the counts of each associated barcode were summed to generate a cumulative count for that mutant.

Determination of Selection Coefficient. The ratio of the frequency of each variant in the library relative to wild type (ancAmoHsp90 or ScHsp90) was determined at each time point, and the slope of the logarithm of this ratio versus time (in number of generations) was determined as the raw per-generation selection coefficient (s) (20):

$$s = d/dt[\ln(n_m/n_{wt})],$$

where n_m and n_{wt} are the number of sequence reads of mutant and wild type, respectively, and time is measured in number of wild-type generations. No-insert plasmid selection coefficients were determined from the first three time points because their counts drop rapidly over time. Mutants with selection coefficients within 3 SDs of the mean of no-insert variants were considered null-like and also analyzed based on the first three time points. For all other variants, selection coefficients were determined from all time points. Final selection coefficients for each variant were scaled in relative fitness space ($w = e^s$) such that the Hsp90-null allele, which is lethal, has a relative fitness of 0 ($s = -\infty$). This definition of relative fitness, unlike that which defines $w = 1 - s$, has the advantage of making selection coefficients additive and reversible (the selection coefficient of mutation from state i to j is the opposite of the selection coefficient of that from j to i) (21).

Generation of Individual Mutants and Monoculture Analysis of Yeast Growth. To measure the relative fitness of ancAscoHsp90, mutations missed in the bulk libraries, and genotypes in mutant cycles that we sought to test in combination for epistatic interactions, we assayed growth rate in monoculture and related this to fitness, which assumes the relative rate of growth of two genotypes is the same in isolation as in direct competition (20). The growth rate of individually cloned mutants was estimated over 30 h of growth with periodic dilution to maintain log-phase growth, as per Jiang et al. (15). Growth rates were determined as the slope of the linear model relating the log-transformed dilution-corrected cell density to time. The growth rate was converted to an estimate of the selection coefficient by taking the difference in growth rate (Malthusian parameter) between mutant and wild type and multiplying this by the wild-type generation time (20), and then

rescaling selection coefficients in relative fitness space such that a null mutant analyzed in parallel has relative fitness 0 ($s = -\infty$).

Individual mutants of ancAmoHsp90 and ScHsp90 were generated in the p414ADHΔTer background by QuikChange site-directed mutagenesis (Dataset S9), confirmed by Sanger sequencing. Mutations that were generated and assayed in ancAmoHsp90 (with number of replicate measurements in parentheses) include the following: S49A ($n = 1$), T137I ($n = 1$), V147I ($n = 1$), I158V ($n = 1$), R160L ($n = 1$), G164N ($n = 1$), E165P ($n = 1$), L167I ($n = 1$), K172I ($n = 1$), L193I ($n = 1$), and V194I ($n = 1$). Mutations generated and assayed in ScHsp90 include the following: T5S ($n = 3$), E7A ($n = 4$), T13N ($n = 3$), V23F ($n = 2$), N151A ($n = 3$), and L378I ($n = 2$); double mutants E7A/T13N ($n = 3$), E7A/N151A ($n = 3$), T13N/N151A ($n = 3$), V23F/T13N ($n = 1$), V23F/N151A ($n = 1$), E7A/L378I ($n = 1$), and V23F/L378I ($n = 1$); and triple mutants E7A/T13N/N151A ($n = 2$) and V23F/T13N/N151A ($n = 1$).

Robustness of Results to Statistical Uncertainty and Technical Variables. The conclusion that the typical ancestral state is deleterious in ScHsp90 is robust to the exclusion of 20 ancestral states that have posterior probability <1.0 at all ancestral nodes along the trajectory ($P = 4.5 \times 10^{-14}$, Wilcoxon rank sum test with continuity correction). The mutation to one ancestral state was missed in the bulk competition: its selection coefficient was inferred separately via monoculture, and including it in the analysis still leads to the conclusion that the typical ancestral state is deleterious ($P = 7.8 \times 10^{-17}$, Wilcoxon rank sum test with continuity correction).

The conclusion that the average derived state is deleterious in ancAmoHsp90 is retained when we include only the 32 mutations for which the ancAmoHsp90 state is inferred with a posterior probability of 1.0 and the derived state is inferred with posterior probability 1.0 in at least one node along the trajectory ($P = 1.1 \times 10^{-4}$, Wilcoxon rank sum test with continuity correction). The conclusion is also robust if we include selection coefficients as determined separately via monoculture for mutations to 11 derived states that were missed in the bulk competition ($P = 5.4 \times 10^{-4}$, Wilcoxon rank sum test with continuity correction).

We assessed relative fitness for six genotypes (ScHsp90+E7a, ScHsp90+V23f, ScHsp90+N151a, ScHsp90+T13n, ancAmoHsp90, and ancAmoHsp90+i378L) both by monoculture and by bulk competition. These two measures are well correlated (Pearson $R^2 = 0.95$), although the magnitude of a fitness effect is smaller when measured by monoculture growth assays (Fig. S3F), perhaps because of differences in experimental conditions for bulk versus monoculture growth, such as the type of growth vessel and culture volume (and consequential aeration). The only conclusion involving a comparison between these two kinds of measurements is that ancAscoHsp90 (measured via monoculture) is more fit than would be predicted from the sum of selection coefficients of its component states (measured via bulk competition) (Fig. 2 and Fig. S7). We therefore used the observed linear relationship between the two types of fitness assays to transform ancAscoHsp90's fitness as measured by monoculture (0.991); the expected fitness of ancAscoHsp90 in a bulk competition is 0.986, still much larger than the predicted fitness of 0.65 in the absence of epistasis.

Expected Versus Observed Fitness. To identify epistasis between candidate interacting sites (e.g., Fig. 4) or among the broader set of substitutions (e.g., Fig. 2), we compared the observed fitness of genotypes with multiple mutations to that expected in the absence of epistasis. In the absence of epistatic interactions, selection coefficients combine additively (21). We therefore calculated the expected selection coefficient of a genotype as the sum of selection coefficients of its component mutations as measured independently in a reference background (ancAmoHsp90 or

values for SEM_{wt} and SEM_{mut} were similar (0.0040 and 0.0041, respectively). The posterior probability that a variant is nonneutral is calculated from the relative likelihoods of the two hypotheses, with a uniform prior on the two hypotheses:

$$P(\text{nonneutral}) = \frac{P(s_{\text{obs}} | s \sim N(s_{\text{obs}}, SEM_{\text{mut}}))}{P(s_{\text{obs}} | s \sim N(s_{\text{obs}}, SEM_{\text{mut}})) + P(s_{\text{obs}} | s \sim N(0, SEM_{\text{wt}}))}.$$

If a variant has $s_{\text{obs}} > 0$, then $P(\text{nonneutral})$ corresponds to a probability that a mutation is beneficial; if a variant has $s_{\text{obs}} < 0$, then $P(\text{nonneutral})$ corresponds to a probability that a mutant is deleterious. To estimate the proportion of mutations that are in each fitness category, we summed the probabilities for each category across all mutants.

Last, we constructed a 95% CI for each mutation given its mean selection coefficient and the estimated SEM_{mut} described above. We then counted the fraction of mutations that are below (or above) zero and whose 95% CI excludes zero. This yields a

conservative estimate for our parameter of interest, the total fraction of mutations that are deleterious (or beneficial), as it is designed to indicate whether any particular mutation is deleterious (or beneficial), not to estimate the proportion (which does not depend on unequivocally classifying any one individual mutation as neutral or not).

- Adl SM, et al. (2012) The revised classification of eukaryotes. *J Eukaryot Microbiol* 59: 429–493.
- Pantartz CN, Drosopoulou E, Scouras ZG (2013) Assessment and reconstruction of novel HSP90 genes: duplications, gains and losses in fungal and animal lineages. *PLoS One* 8:e73217.
- Li W, Godzik A (2006) Cd-hit: a fast program for clustering and comparing large sets of protein or nucleotide sequences. *Bioinformatics* 22:1658–1659.
- Sievers F, et al. (2011) Fast, scalable generation of high-quality protein multiple sequence alignments using Clustal Omega. *Mol Syst Biol* 7:539.
- Le SQ, Gascuel O (2008) An improved general amino acid replacement matrix. *Mol Biol Evol* 25:1307–1320.
- Stamatakis A (2014) RAxML version 8: a tool for phylogenetic analysis and post-analysis of large phylogenies. *Bioinformatics* 30:1312–1313.
- Brown MW, et al. (2013) Phylogenomics demonstrates that breviate flagellates are related to opisthokonts and apusomonads. *Proc Biol Sci* 280:20131755.
- Brown MW, Spiegel FW, Silberman JD (2009) Phylogeny of the “forgotten” cellular slime mold, *Fonticula alba*, reveals a key evolutionary branch within Opisthokonta. *Mol Biol Evol* 26:2699–2709.
- Paps J, Medina-Chacón LA, Marshall W, Suga H, Ruiz-Trillo I (2013) Molecular phylogeny of unikonts: new insights into the position of apusomonads and ancyromonads and the internal relationships of opisthokonts. *Protist* 164:2–12.
- Kurtzman CP, Robnett CJ (2013) Relationships among genera of the Saccharomycotina (Ascomycota) from multigene phylogenetic analysis of type species. *FEMS Yeast Res* 13:23–33.
- Shen X-X, et al. (2016) Reconstructing the backbone of the Saccharomycotina yeast phylogeny using genome-scale data. *G3 (Bethesda)* 6:3927–3939.
- Yang Z, Kumar S, Nei M (1995) A new method of inference of ancestral nucleotide and amino acid sequences. *Genetics* 141:1641–1650.
- Ali MMU, et al. (2006) Crystal structure of an Hsp90-nucleotide-p23/Sba1 closed chaperone complex. *Nature* 440:1013–1017.
- Cunningham CN, Southworth DR, Krukenberg KA, Agard DA (2012) The conserved arginine 380 of Hsp90 is not a catalytic residue, but stabilizes the closed conformation required for ATP hydrolysis. *Protein Sci* 21:1162–1171.
- Jiang L, Mishra P, Hietpas RT, Zeldovich KB, Bolon DNA (2013) Latent effects of Hsp90 mutants revealed at reduced expression levels. *PLoS Genet* 9:e1003600.
- Hiatt JB, Patwardhan RP, Turner EH, Lee C, Shendure J (2010) Parallel, tag-directed assembly of locally derived short sequence reads. *Nat Methods* 7:119–122.
- Hietpas RT, Bank C, Jensen JD, Bolon DNA (2013) Shifting fitness landscapes in response to altered environments. *Evolution* 67:3512–3522.
- Mishra P, Flynn JM, Starr TN, Bolon DNA (2016) Systematic mutant analyses elucidate general and client-specific aspects of Hsp90 function. *Cell Reports* 15:588–598.
- Hietpas R, Roscoe B, Jiang L, Bolon DNA (2012) Fitness analyses of all possible point mutations for regions of genes in yeast. *Nat Protoc* 7:1382–1396.
- Chevin LM (2011) On measuring selection in experimental evolution. *Biol Lett* 7:210–213.
- Sella G, Hirsh AE (2005) The application of statistical physics to evolutionary biology. *Proc Natl Acad Sci USA* 102:9541–9546.
- Benaglia T, Chauveau D, Hunter D (2009) mixtools: An R package for analyzing finite mixture models. *J Stat Softw* 32.

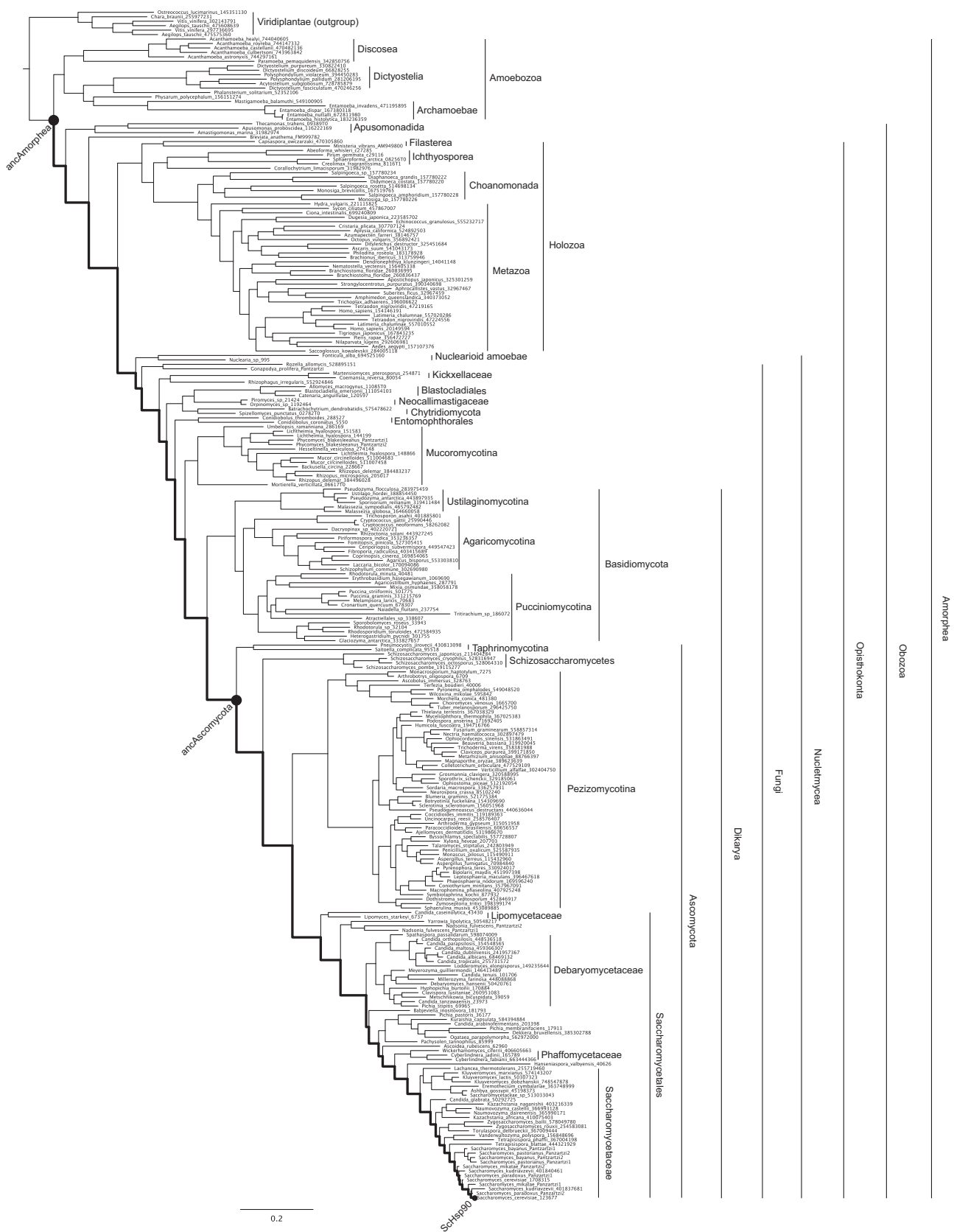


Fig. S1. Hsp90 phylogeny. The ML phylogeny of 267 Hsp90 protein sequences, with major taxonomic groups labeled. Taxon names indicate genus, species, and an accession number or sequence identifier; complete sequence identification information is given in Dataset S3. Nodes characterized in this study are shown as black dots; the trajectory studied is shown as a thick black line.

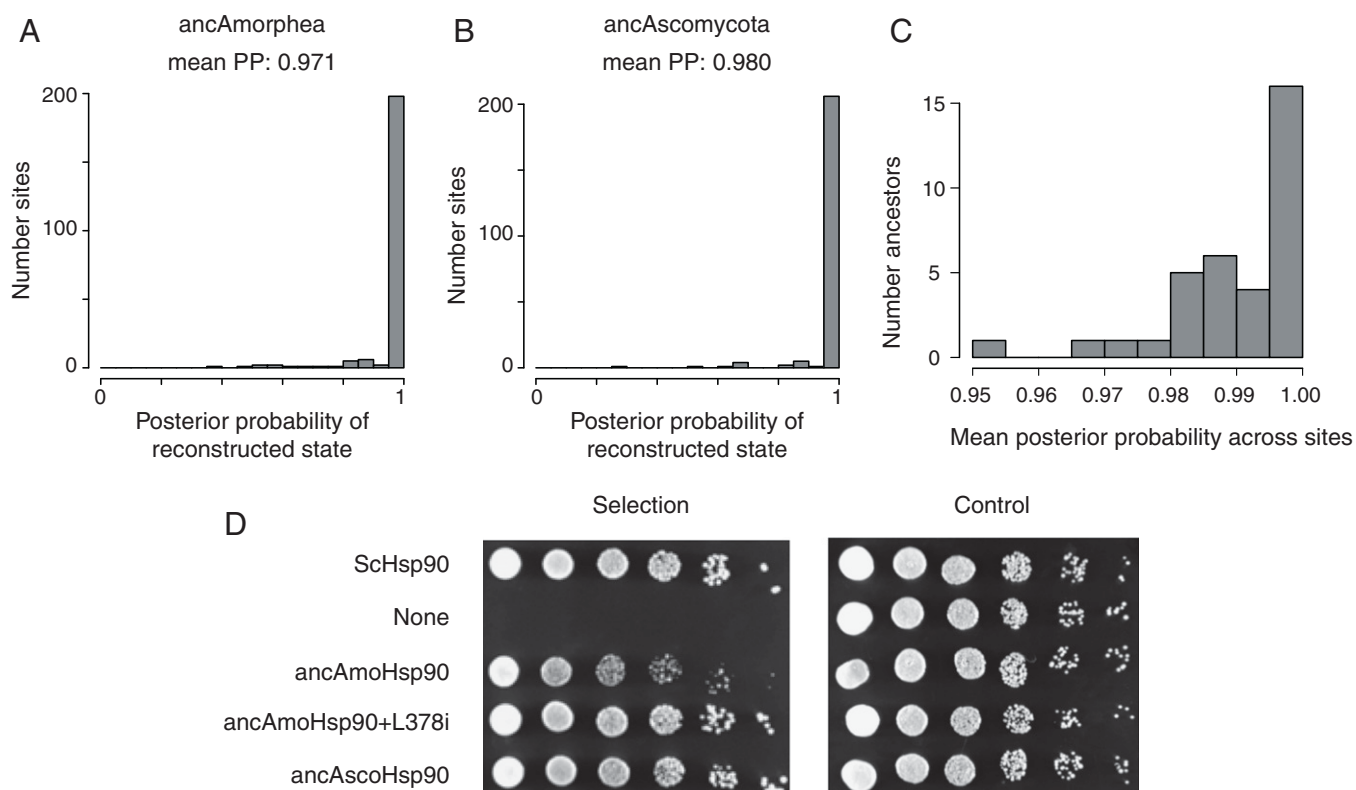


Fig. S2. Ancestral Hsp90 sequences have high statistical support and complement yeast growth. (A and B) For the ancestral NTD sequences reconstructed in this study, the distribution of posterior probability of ancestral states across NTD sites is shown as a histogram. The mean posterior probability of the most probable state across sites (mean PP) is shown for each ancestor. (C) The distribution of mean PP for all reconstructed ancestral sequences along the trajectory from ancAmoHsp90 to ScHsp90. (D) Growth of *S. cerevisiae* Hsp90 shutoff strains complemented with ancestral Hsp90 NTD variants. Spots from Left to Right are fivefold serial dilutions. Control plates represent conditions in which the native ScHsp90 allele is expressed. Under selection conditions, the native ScHsp90 allele is turned off, and growth can only persist when a complementary Hsp90 allele is provided. The ancAmoHsp90 NTD expressed as a chimera with the Sc middle and C-terminal domains exhibits a slight growth defect; this is rescued by adding an additional reversion to the ancAmoHsp90 state in the middle domain (L378i), which occurs on a middle domain loop that extends down and interacts directly with the N-terminal domain and contributes to the NTD ATP-binding pocket. We subsequently refer to ancAmoHsp90+L378i as ancAmoHsp90.

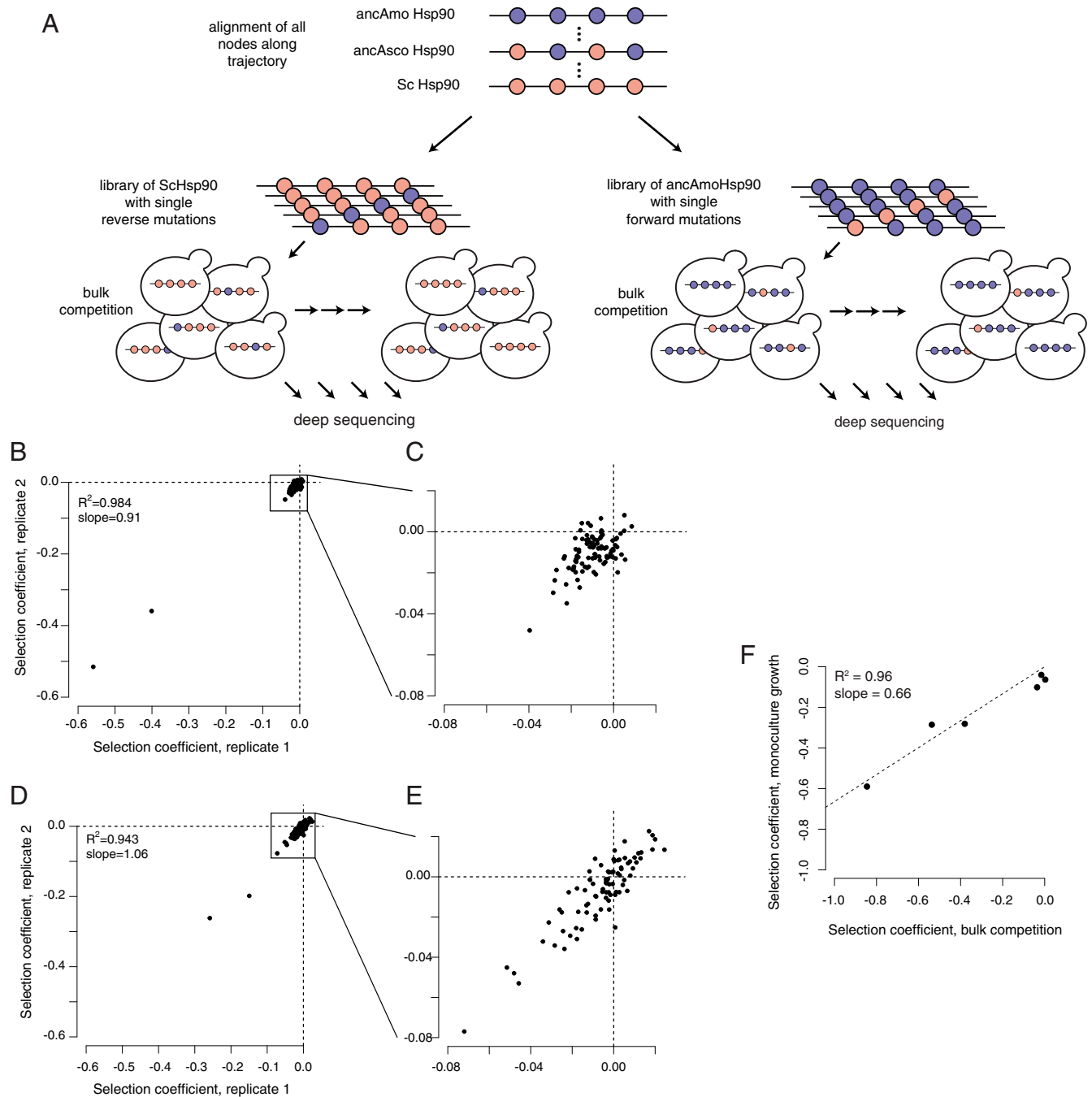


Fig. S3. Experimental scheme and reproducibility. (A) Experimental scheme for testing the fitness effects of individual mutations to ancestral states in ScHsp90 (Left) or individual mutations to derived states in ancAmoHsp90 (Right). An alignment of all ancestors along the focal trajectory was constructed to identify the trajectory of Hsp90 NTD sequence change from ancAmoHsp90 to ScHsp90. In the ScHsp90 and ancAmoHsp90 backgrounds, libraries were constructed consisting of the wild-type sequence and all individual mutations to ancestral or derived states. These libraries were transformed into yeast, which grew through a bulk competition. The frequency of each genotype at each time point was determined by deep sequencing, allowing us to calculate a selection coefficient for each mutation relative to the respective wild-type sequence. (B) Reproducibility in selection coefficient estimates for replicate bulk competitions of the ScHsp90 library. R^2 , Pearson coefficient of determination. (C) For visual clarity, zoomed-in representation of the boxed region in B. (D) Reproducibility in selection coefficient estimates for replicate bulk competitions of the ancAmoHsp90 library. R^2 , Pearson coefficient of determination. (E) For visual clarity, zoomed-in representation of the boxed region in D. (F) Correlation in fitness as measured via bulk competition or monoculture growth assay. R^2 , Pearson coefficient of determination. The line was forced to go through (0, 0); when freely fit, the intercept term was not significantly different from zero.

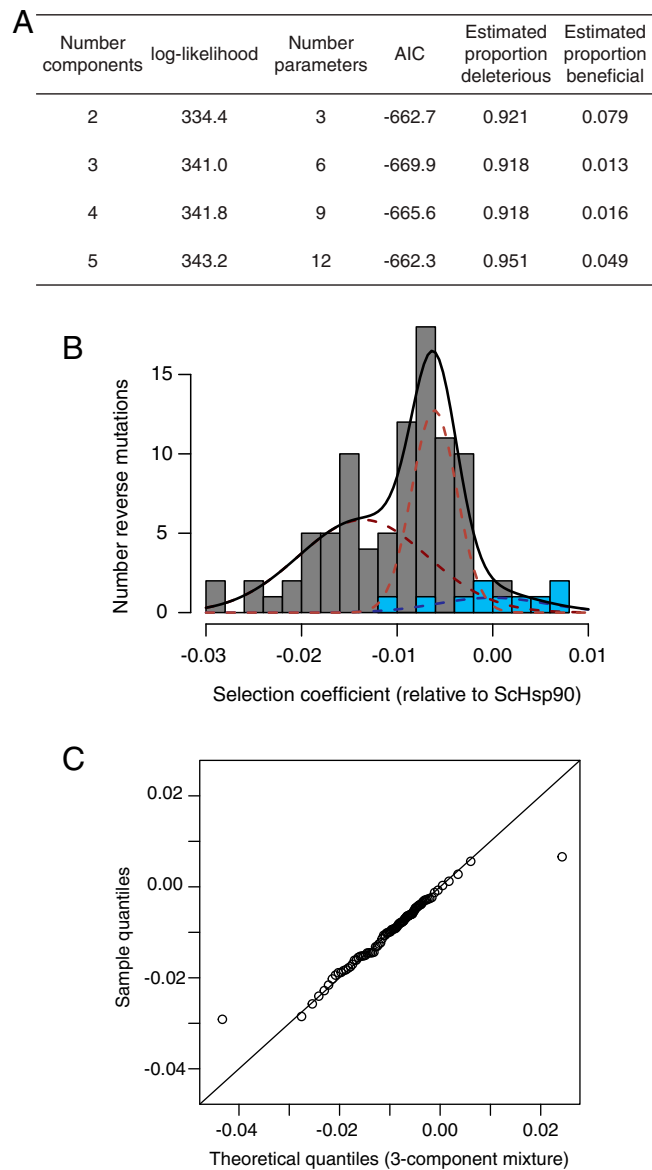


Fig. S4. Estimating the proportion of mutations to ancestral states that are deleterious with a mixture model. (A) Observed selection coefficients of reversions were fit to mixture models containing a variable number of Gaussian distributions; in each case, one neutral mixture component is fixed to have the mean and SD of the sampling distribution of replicate wild-type ScHsp90 sequences present in the library, the mixture proportion of which is a free parameter; each additional nonneutral mixture component has a free mean, SD, and mixture proportion. The empirical data were best fit by a three-component mixture model, as assessed by AIC. Proportion deleterious (or beneficial) was estimated by summing the cumulative density below (or above) zero of the nonneutral components. (B) The best-fit mixture model. Gray bars, observed distribution of selection coefficients of ancestral reversions; blue bars, distribution of observed selection coefficients of wild-type ScHsp90 sequences present in the library. Black line, best-fit mixture model; red dashed lines, individual nonneutral mixture components; blue dashed line, neutral (wild-type) mixture component. The area under the curve for each mixture component corresponds to the proportion it contributes to the overall mixture model. (C) Quantile–quantile plot showing the quality of fit of the three-component mixture model (x axis) to the empirical distribution of selection coefficients of ancestral reversions (y axis). The mixture model assigns more extreme selection coefficients to the tails than is observed in the empirical distribution but provides a reasonable fit along the bulk of the distribution.

A

Method	Proportion deleterious, Sc	Proportion neutral, Sc	Proportion beneficial, Sc	Proportion deleterious, ancAmo	Proportion neutral, ancAmo	Proportion beneficial, ancAmo
Mixture model	0.92	0.07	0.01	0.48	0.32	0.20
Count	0.95	0.00	0.05	0.66	0.00	0.34
Empirical Bayes	0.81	0.16	0.03	0.55	0.19	0.27
Confidence Interval	0.54	0.45	0.01	0.48	0.26	0.26

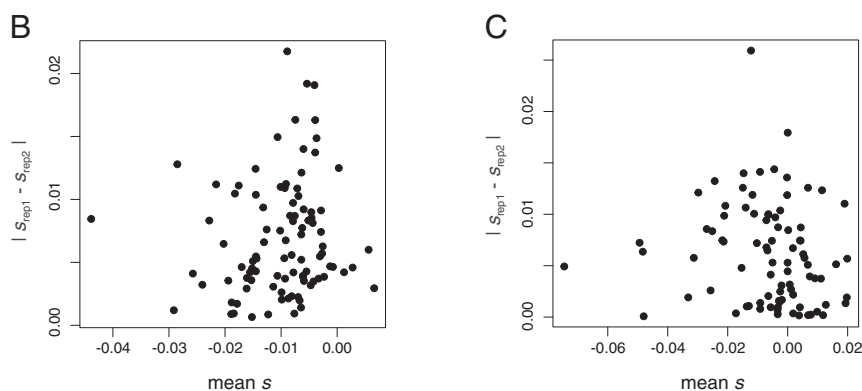


Fig. S55. Alternate approaches for estimating the proportion of mutations that are deleterious. (A) The estimated proportion of mutations that are deleterious, neutral, or beneficial in each background, as determined by each of four statistical methods. See *SI Methods* for descriptions of each method. (B and C) Experimental errors are unbiased with respect to the observed selection coefficient. For the ScHsp90 (B) and ancAmoHsp90 (C) backgrounds, the absolute difference in s as determined in each replicate is shown versus their mean. In each background, there is no significant linear relationship between experimental error and s_{obs} ($P = 0.27$ and 0.24 , respectively; Pearson's correlation).

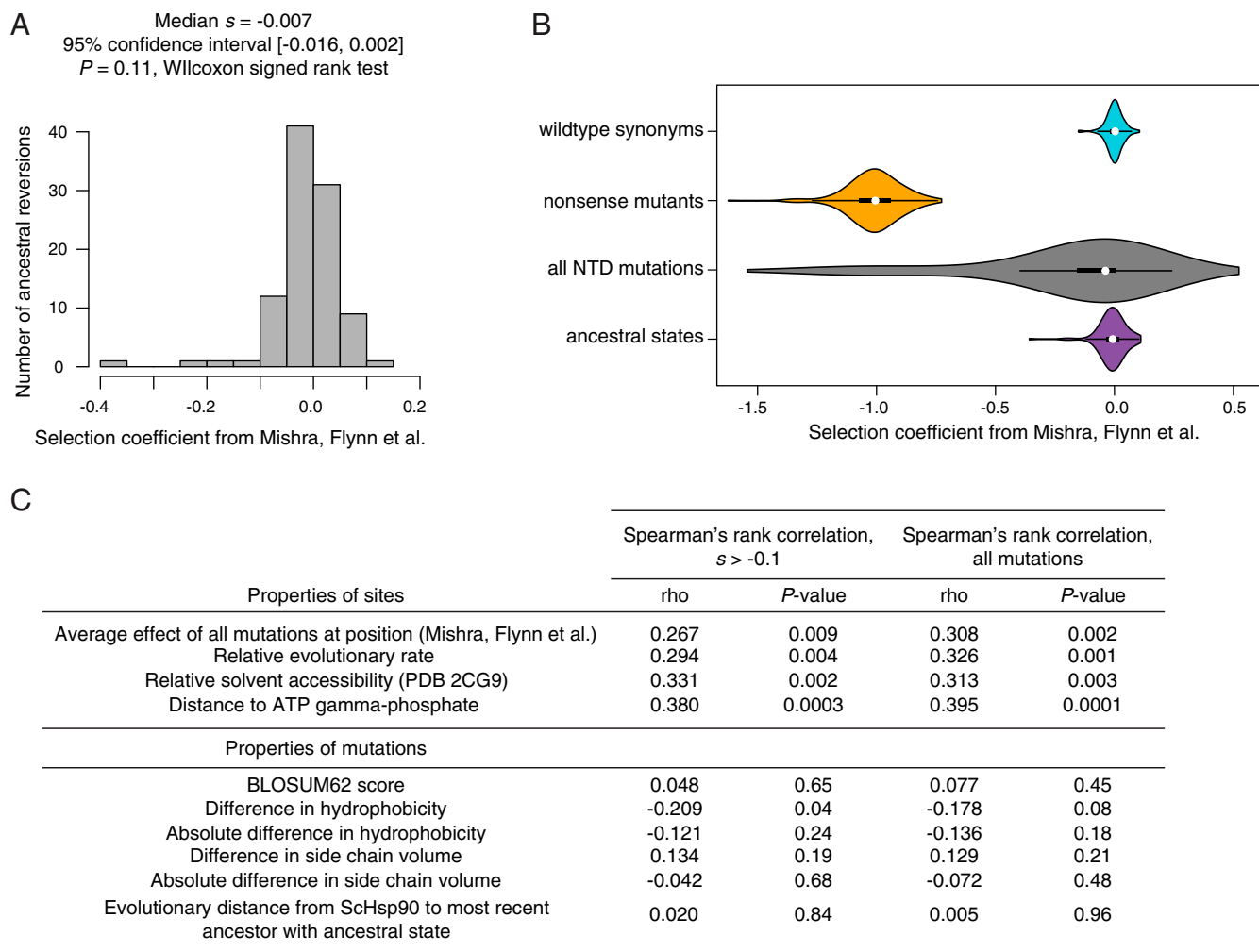


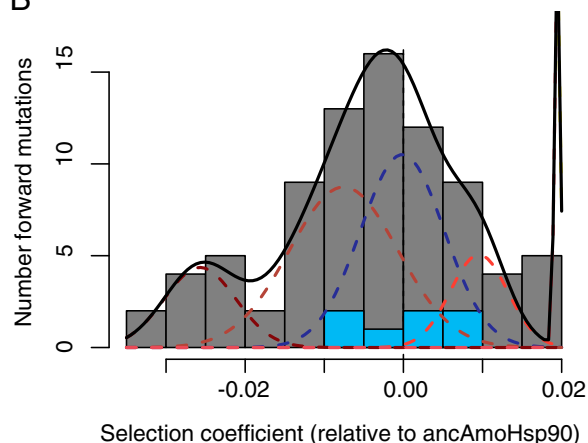
Fig. S6. Ancestral states are deleterious in yeast Hsp90. (A) The signature of deleterious ancestral states is present in the independent but lower-resolution dataset of Mishra et al. (1). For each mutation to an ancestral state, the selection coefficient as determined by Mishra et al. is shown. The median selection coefficient is -0.007 , close to that estimated in the current study; however, this median selection coefficient is not significantly different from zero ($P = 0.11$). Because Mishra et al. tested a much larger panel of mutations (all single mutations across the entire NTD), experimental variability of estimated selection coefficients was much larger, possibly explaining the lack of significance of this result in this dataset. (B) Violin plots show the distribution of mutant effects in the dataset of Mishra et al. (1). Ancestral states are less detrimental than the average random mutation in the NTD ($P = 3.5 \times 10^{-9}$, Wilcoxon rank sum test with continuity correction). (C) Reversions exhibit properties typical of genuinely deleterious mutations. For various properties of sites at which we measured the fitness of ancestral variants (Top) or properties of the specific amino acids mutated (Bottom), we asked whether there was a significant correlation between the property and the selection coefficients of mutations via Spearman's rank correlation. Ancestral states tend to be more deleterious at positions that are less robust to any mutation, evolve more slowly, are less solvent accessible, and are closer to the γ -phosphate of bound ATP. These properties are not completely independent; for example, there is a significant positive correlation between relative solvent accessibility and distance to ATP γ -phosphate. Biochemical properties particular to the amino acid states in each mutation are generally not significantly correlated with the selective effect. Furthermore, in contrast to previous observations, we see no evidence for older states being more entrenched (2–4).

1. Mishra P, Flynn JM, Starr TN, Bolon DNA (2016) Systematic mutant analyses elucidate general and client-specific aspects of Hsp90 function. *Cell Reports* 15:588–598.
2. Pollock DD, Thiltgen G, Goldstein RA (2012) Amino acid coevolution induces an evolutionary Stokes shift. *Proc Natl Acad Sci USA* 109:E1352–E1359.
3. Shah P, McCandlish DM, Plotkin JB (2015) Contingency and entrenchment in protein evolution under purifying selection. *Proc Natl Acad Sci USA* 112:E3226–E3235.
4. Soylemez O, Kondrashov FA (2012) Estimating the rate of irreversibility in protein evolution. *Genome Biol Evol* 4:1213–1222.

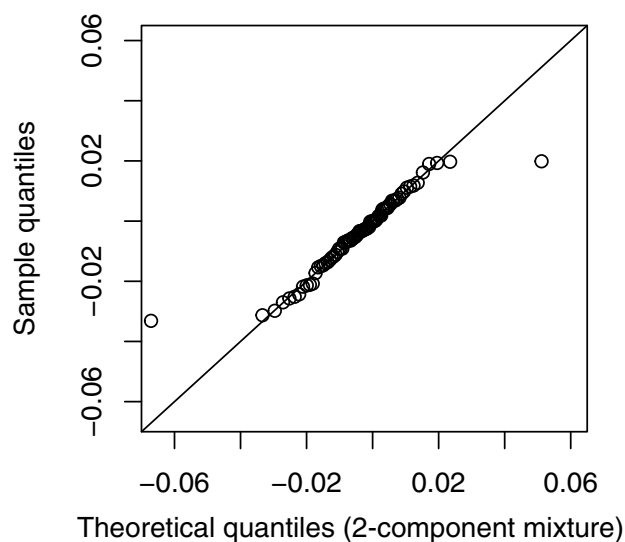
A

Number components	log-likelihood	Number parameters	AIC	Estimated proportion deleterious	Estimated proportion beneficial
2	243.9	3	-481.7	0.532	0.250
3	245.5	6	-479.0	0.587	0.330
4	246.2	9	-474.4	0.412	0.132
5	252.7	12	-481.5	0.482	0.197
6	252.7	15	-475.5	0.482	0.197

B



C



D

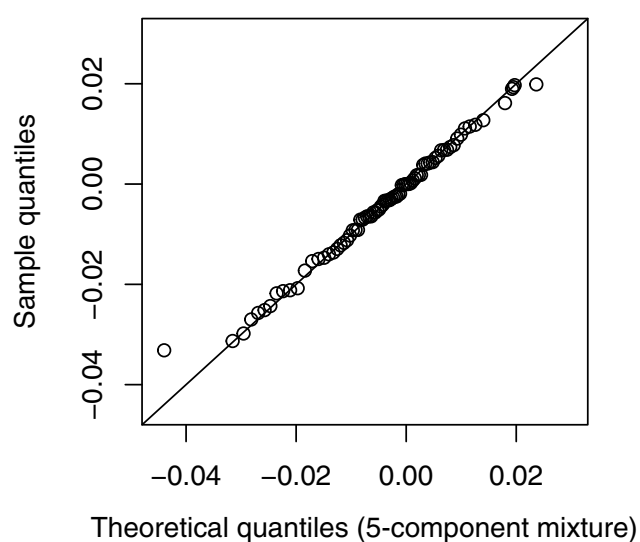
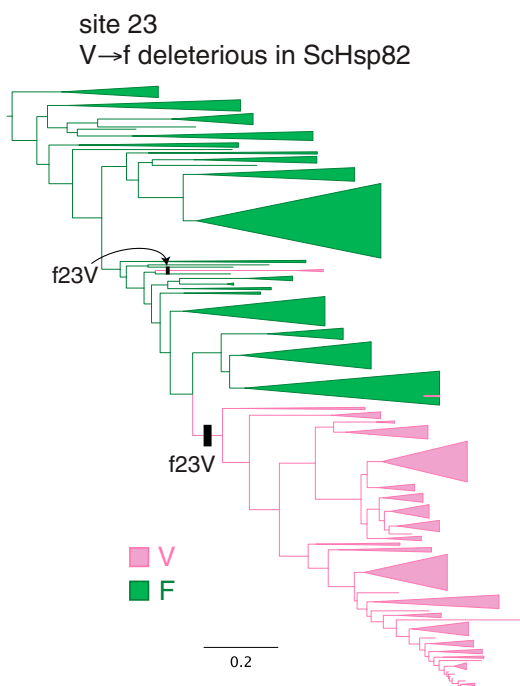
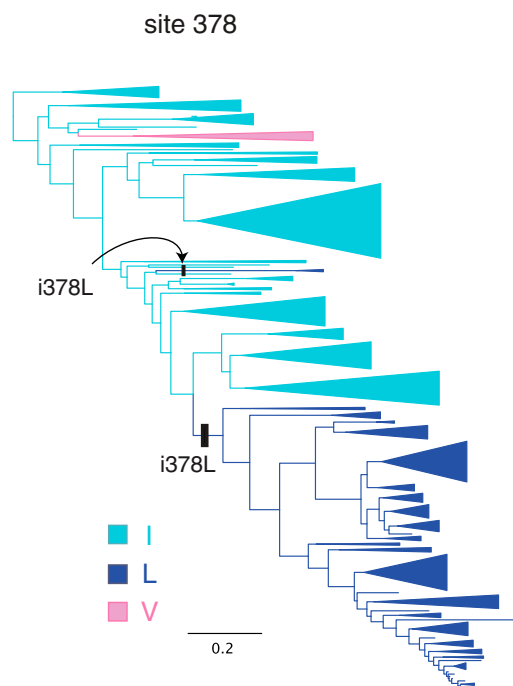


Fig. S8. Estimating the proportion of mutations to derived states that are deleterious with a mixture model. (A) The distribution of selection coefficients of mutations to derived states was fit by mixture models containing a variable number of Gaussian distributions; in each case, one neutral mixture component is fixed to have the mean and SD of the sampling distribution of replicate wild-type *ancAmoHsp90* alleles in the library, the mixture proportion of which is a free parameter; each additional nonneutral mixture component has a free mean, SD, and mixture proportion. The empirical data were best fit by a two-component mixture model, as judged by AIC, with a five-component mixture being almost equally well fit; the five-component mixture resulted in a more conservative estimate of the proportion of mutations that were deleterious than the two-component mixture, and so was chosen despite the AIC difference of 0.2. Proportion deleterious (or beneficial) was estimated by summing the cumulative density below (or above) zero of the nonneutral components. (B) The fit of the five-component mixture model. Gray bars, distribution of selection coefficients of mutations to derived states; blue bars, distribution of selection coefficients of independent *ancAmoHsp90* alleles present in the library. Black line, five-component mixture model; red dashed lines, individual nonneutral mixture components; blue dashed line, neutral (wild-type) mixture component. The area under the curve for each mixture component corresponds to the proportion it contributes to the overall mixture model. (C and D) Quantile–quantile plot showing the quality of fit of the two-component (C), or five-component (D), mixture models (x axis) to the empirical distribution of selection coefficients of mutations to derived states (y axis).

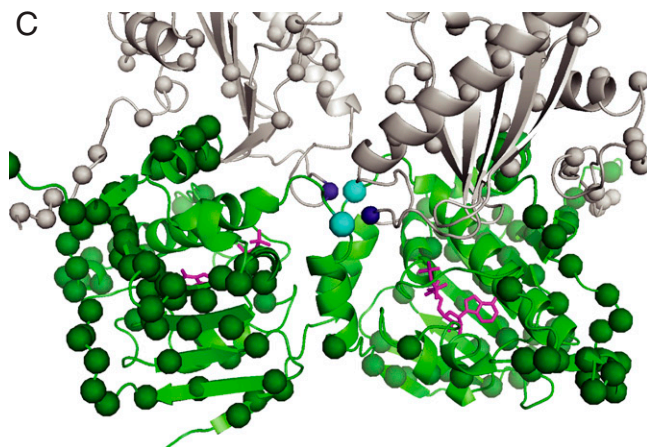
A



B



C



D

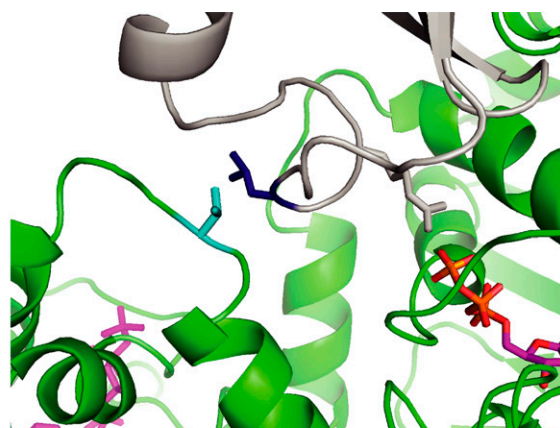


Fig. S9. The deleterious V23f reversion is ameliorated by L378i. (A and B) Character state patterns at sites 23 (A) and 378 (B). On the lineage to ScHsp90, f23V co-occurred with i378L before the common ancestor of Ascomycota. The same two substitutions also co-occur on an independent lineage on this phylogeny (Kickxellaceae fungi), and in the distantly related Rhodophyta red algae (GenBank ADB45333.1 and RefSeq XP_005715129.1). (C) The locations of sites 23 and 378 on the ATP-bound Hsp90 dimer structure (PDB ID code 2CG9). Cyan spheres, site 23; dark blue; site 378; dark green, other variable NTD sites; gray, other variable middle and C-terminal domain sites. Magenta sticks, ATP. (D) Zoomed view of sites 23 and 378. These side chains are in direct structural contact and may be important for the positioning of the middle domain loop that bears R380 (gray sticks), which forms a salt bridge with the ATP γ -phosphate and is critical for ATP binding and hydrolysis (1, 2).

1. Ali MMU, et al. (2006) Crystal structure of an Hsp90-nucleotide-p23/Sba1 closed chaperone complex. *Nature* 440:1013–1017.
2. Cunningham CN, Southworth DR, Krukenberg KA, Agard DA (2012) The conserved arginine 380 of Hsp90 is not a catalytic residue, but stabilizes the closed conformation required for ATP hydrolysis. *Protein Sci* 21:1162–1171.

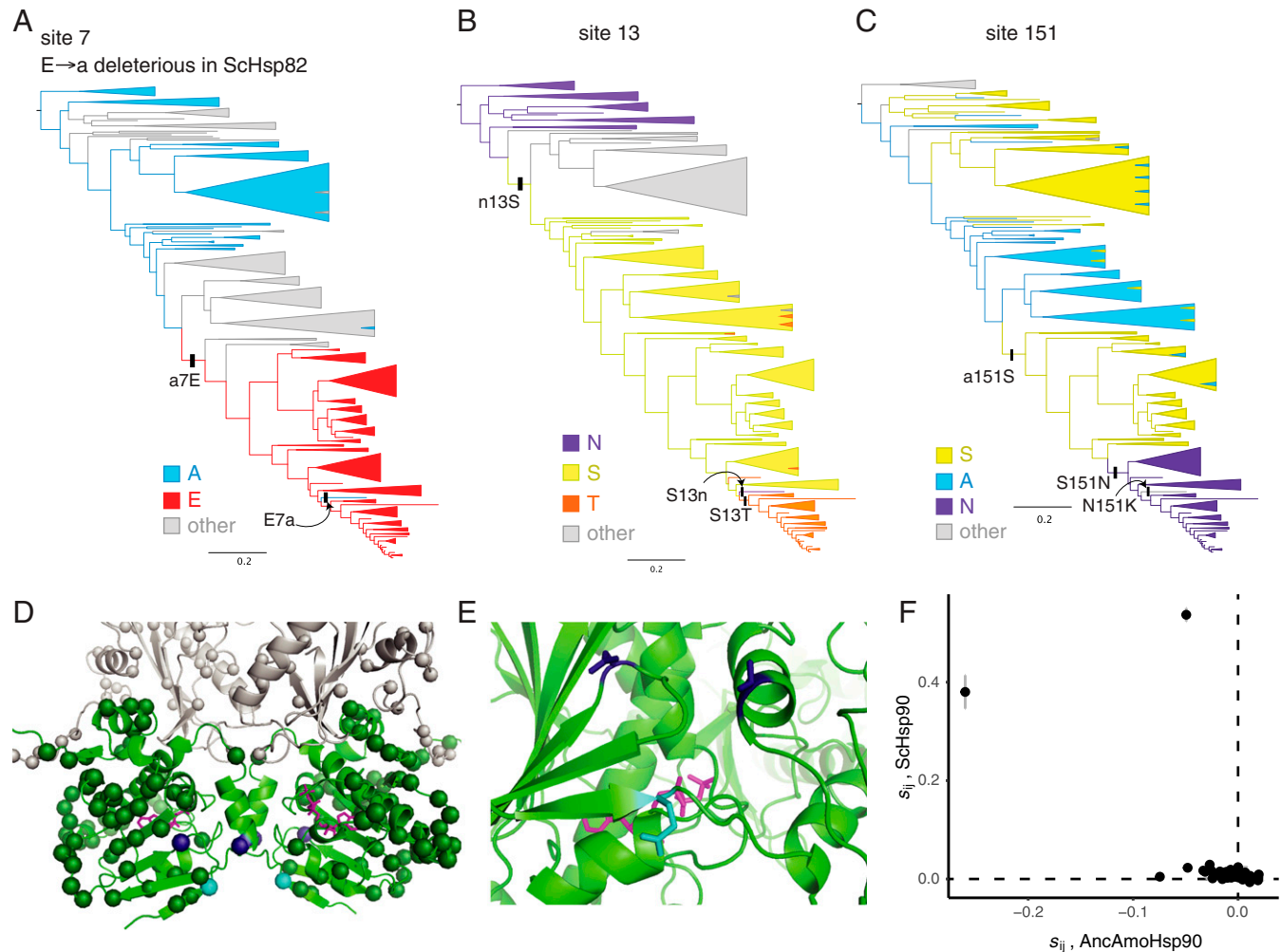


Fig. S10. The deleterious E7a reversion is partially ameliorated by N151a or T13n. (A–C) Character state patterns at sites 7 (A), 13 (B), and 151 (C). On the trajectory to SchSp90, a7E occurred before the common ancestor of Ascomycota, then later reverted in the lineage leading to *Ascoidea rubescens* (arrow); on this latter lineage, site 13 also reverted to the ancestral state asparagine, and site 151 substituted to a third state lysine. (D) The locations of sites 7, 13, and 151 on the ATP-bound Hsp90 structure (2CG9), represented as in Fig. S9C. Cyan spheres, site 7; dark blue, sites 13 and 151. (E) Zoomed-in view of sites 7, 13, and 151. These side chains are not in direct physical contact; however, site 7 is on a β -strand that undergoes extensive conformational movement when Hsp90 converts between ADP- and ATP-bound states. (F) The same plot as Fig. 5C is shown, including the two strong outliers V23f and E7a. See Fig. 5C legend for details.

Other Supporting Information Files

[Dataset S1 \(TXT\)](#)
[Dataset S2 \(TXT\)](#)
[Dataset S3 \(XLSX\)](#)
[Dataset S4 \(TXT\)](#)
[Dataset S5 \(CSV\)](#)
[Dataset S6 \(CSV\)](#)
[Dataset S7 \(CSV\)](#)
[Dataset S8 \(CSV\)](#)
[Dataset S9 \(XLSX\)](#)